

# Contrasting magnetic behavior in $\text{MnSc}_2\text{X}_4$ ( $X = \text{S}, \text{Se}$ ) spinel compounds investigated by magnetoelastic studies

J. Grumbach,<sup>1,\*</sup> J. Sourd,<sup>2</sup> M. Deeb,<sup>1</sup> A. Miyata,<sup>2,3</sup> H. Suwa,<sup>4</sup> T. Gottschall,<sup>2</sup> A. Hauspurg,<sup>2</sup> S. Chattopadhyay,<sup>2,5</sup> M. Rotter,<sup>6</sup> S. Granovsky,<sup>1</sup> L. Prodan,<sup>7,8</sup> V. Tsurkan,<sup>7,8</sup> S. Zherlitsyn,<sup>2</sup> M. Doerr,<sup>1</sup> and J. Wosnitzer<sup>1,2</sup>

<sup>1</sup>*Institut für Festkörper- und Materialphysik, Technische Universität Dresden, 01062 Dresden, Germany.*

<sup>2</sup>*Hochfeld-Magnetlabor Dresden (HLD-EMFL) and Würzburg-Dresden Cluster of Excellence ct.qmat, Helmholtz-Zentrum Dresden-Rossendorf, 01328 Dresden, Germany.*

<sup>3</sup>*Institute of Solid State Physics, University of Tokyo, Kashiwa, Chiba, 277-8581, Japan*

<sup>4</sup>*Department of Physics, University of Tokyo, Tokyo 113-0033, Japan*

<sup>5</sup>*UGC-DAE Consortium for Scientific Research Mumbai Centre, 246-C CFB, BARC Campus, Mumbai 400085, India.*

<sup>6</sup>*McPhase Project, 01159 Dresden, Germany.*

<sup>7</sup>*Experimentalphysik V, Center for Electronic Correlations and Magnetism, Institute of Physics, University of Augsburg, 86159 Augsburg, Germany.*

<sup>8</sup>*Institute of Applied Physics, Moldova State University, 2028 Chisinau, R. Moldova.*

The spinel compounds  $\text{MnSc}_2\text{X}_4$  are highly frustrated and candidate materials for vortex-like  $3\mathbf{q}$  magnetic states, such as skyrmions, with propagation vectors in the  $[111]$  plane. Because of the strong magnetoelastic coupling, we could extract a refined magnetic  $(H, T)$  phase diagram for  $\text{MnSc}_2\text{S}_4$  from ultrasound and dilatometry measurements. We found a variety of magnetic phases, including the skyrmion phase, which is stable down to lowest temperatures. In comparison, we investigated  $\text{MnSc}_2\text{Se}_4$ , having a larger distance between the magnetic  $\text{Mn}^{3+}$  ions using the same methods. Unlike in  $\text{MnSc}_2\text{S}_4$ , we found no skyrmion phase and overall a lack of sharp anomalies indicative of phase transitions, neither in dilatometry and ultrasound nor in specific heat and ac-susceptibility data. Motivated by our findings, we performed model calculations, which reproduced the experimentally observed magnetostriction and specific-heat results reasonably well.

## I. INTRODUCTION

The class of spinel compounds containing  $\text{Mn}^{3+}$  ions is known to show complex magnetism such as for example spin-spiral or helical ground states, skyrmion phases, or spin-liquid behavior. Most of these phenomena are driven by asymmetric exchange or frustration effects [1]. Moreover, spinels get attraction because of their application potential in spintronics or as multiferroic materials. It should be mentioned that the variation of ions in the usual  $AB_2X_4$  structure, where  $A$  and  $B$  are usually  $3d$  elements and  $X$  is a chalcogenide, can significantly change the magnetism. Therefore, differences are also expected for the chalcogenides  $\text{MnSc}_2\text{X}_4$  with  $X = \text{S}$  and  $\text{Se}$ .

These compounds crystallize in a structure composed of  $\text{MnX}_6$  tetrahedra and  $\text{ScX}_4$  octahedra. The chalcogenide corners are shared and a combination of a Mn-based diamond structure and a Sc-based pyrochlore structure forms the crystal. Depending on which of the two ionic sites is magnetic, spinels exhibit two types of magnetic frustration. (i) If the pyrochlore site is magnetic, nearest neighbors form tetrahedral networks. Therefore, frustration is induced from nearest-neighbor interaction. An example for such a case is  $\text{ZnCr}_2\text{Se}_4$  [2–4]. (ii) With magnetic ions on the diamond site, such as for  $\text{MnSc}_2\text{X}_4$ , the nearest-neighbor interactions  $J_1$  are not frustrated, whereas the next-nearest neighbors, with

interactions  $J_2$ , form frustrated triangles in the  $(111)$  plane (black triangles in Fig. 1). For  $J_2/J_1 > 1/8$ , frustration is strong enough to form several types of helical as well as spiral spin-liquid ground states [5, 6]. This condition is fulfilled by both  $\text{MnSc}_2\text{X}_4$  compounds [7], so that a variety of magnetic states is present due to frustration.

Neutron-scattering experiments suggest antiferromagnetic skyrmion lattices for both compounds [7–10]. The twisting mechanism responsible for the skyrmion texture is induced by frustration, since spinels are centrosymmetric crystals without Dzyaloshinskii-Moriya interactions. In this case, skyrmion phases may appear. The size of such skyrmions is generally small [11, 12].

In zero field below 1.5 K,  $\text{MnSc}_2\text{S}_4$  shows a commensurate helical magnetic structure with a propagation vector  $\mathbf{q} = (3/4, 3/4, 0)$ . Modifications of this magnetic structure can be explained by structural lattice changes [13]. Also, theoretical concepts demonstrated the connection between crystal structure, spin orientation, and frustration in spinel compounds [5, 14]. In particular, the strong spin-lattice coupling in  $\text{MnSc}_2\text{S}_4$  decisively influences the magnetic behavior [15, 16]. These considerations motivated our investigation using lattice-sensitive dilatometry and ultrasonic methods, which are also a powerful tool for detecting magnetic phase transitions.

$\text{MnSc}_2\text{Se}_4$  is less extensively investigated, but is related to  $\text{MnSc}_2\text{S}_4$ , since the chalcogenide  $\text{Se}^{2-}$  is only expanding the distances of the magnetic ions, without changing their magnetic moment or the lattice symmetry [18]. Previous results showed similarities to  $\text{MnSc}_2\text{S}_4$ . Neutron-scattering results indicated a putative helical

\* E-Mail: Justus.Grumbach@tu-dresden.de

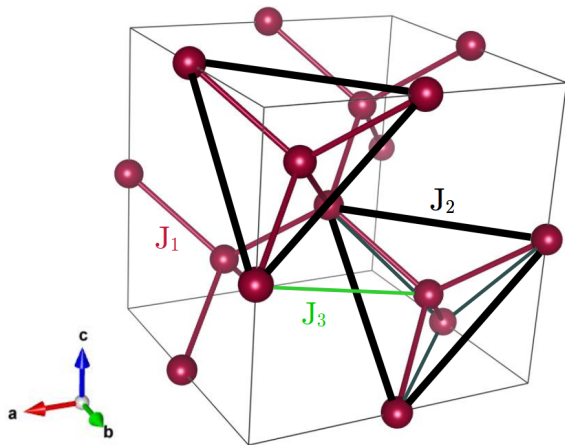


FIG. 1. Crystal structure of  $\text{MnSc}_2\text{X}_4$  with cubic unit cell. Only the magnetic Mn sites are shown. These are located so that next-nearest neighbors are arranged in triangular planes perpendicular to the  $[111]$  direction.  $J_1$ ,  $J_2$ , and  $J_3$  represent the magnetic exchange interactions between nearest, next-nearest, and third-nearest neighbors, respectively. The visualization was done using VESTA [17].

ground state with the same propagation vector  $\mathbf{q} = (3/4, 3/4, 0)$  [7]. In addition, ac-susceptibility measurements revealed three transitions around 2 K. Our scope was to map out the magnetic-field-temperature phase diagram of this compound, compare the results of both compounds, and better understand the link between possible skyrmions, frustration, and magnetoelastic couplings.

## II. EXPERIMENTAL

Single crystals of  $\text{MnSc}_2\text{X}_4$  ( $X = \text{S}, \text{Se}$ ) with face-centered cubic structure (space group  $Fd\bar{3}m$ ) were grown by chemical transport reaction, using iodine as the transport agent. We confirmed the formation of the normal cubic spinel structure by powder x-ray diffraction on crushed single crystals. Both crystals,  $\text{MnSc}_2\text{S}_4$  and  $\text{MnSc}_2\text{Se}_4$ , were of the same purity and quality, as indicated by the powder x-ray diffraction patterns already published in [19] and the supplement to [20]. We performed magnetic characterization by SQUID magnetometry and compared the results to that of stoichiometric powder samples. A more detailed description of the crystal growth and characterization can be found in Refs. [8, 20]. We cut pieces with the required orientation optimized for ultrasound as well as for dilatometry measurements with a characteristic length of 1 to 3 mm from large crystals. The dimensions of the  $\text{MnSc}_2\text{S}_4$  crystal were  $2.2 \times 2.2 \times 1.2 \text{ mm}^3$  and  $1.65 \times 1.65 \times 0.85 \text{ mm}^3$  for the  $\text{MnSc}_2\text{Se}_4$  crystal.

We performed measurements of the magnetostriction and thermal expansion parallel to the crystallographic  $[111]$  direction with magnetic fields oriented in the same

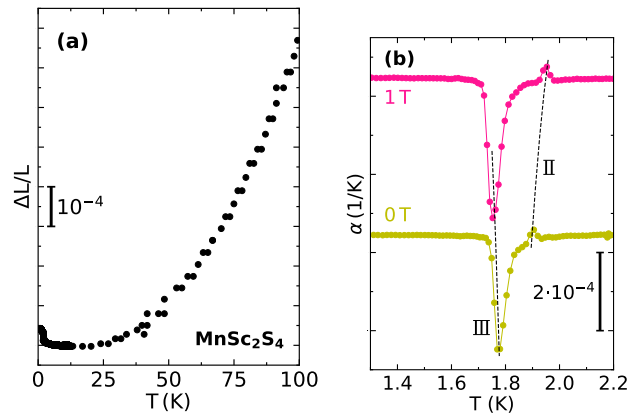


FIG. 2. (a) Thermal-expansion data of  $\text{MnSc}_2\text{S}_4$  up to 100 K. (b) Low-temperature thermal-expansion coefficient  $\alpha$  in 0 and 1 T.

direction. We used a commercial capacitive dilatometer cell [21] placed in a  $^3\text{He}$  cryostat equipped with an 18/20 T magnet. We chose field-sweep rates between 0.05 and 0.25 T/min. The resolution in relative length changes,  $\Delta L/L$ , was about  $10^{-7}$ .

In addition, we performed ultrasound experiments in the same cryostat, using a transmission pulse-echo technique with phase-sensitive detection [22, 23]. We attached  $\text{LiNbO}_3$  transducers ( $36^\circ$ -Y cut for exciting longitudinal modes) to the polished surfaces of the single crystals. We applied magnetic fields up to 18 T so that the ultrasound propagation direction  $\mathbf{k}$  was aligned parallel to the magnetic field  $\mathbf{k} \parallel \mathbf{H} \parallel [111]$ .

Further, we performed ac-susceptibility measurements down to 1.6 K using a standard induction setup in a  $^4\text{He}$  flow cryostat. We used frequencies from 500 Hz to 3 kHz and temperature sweep rates of 0.1 to 0.5 K/min.

We determined the specific heat using the quasi-adiabatic heat-pulse method [24]. For this, we mounted the sample on a sapphire platform with a calibrated Cernox thermometer in a  $^3\text{He}$  sorb-pumped cryostat. We measured the heat capacity of the platform and the grease separately and subtracted it to determine the specific heat of the sample.

## III. EXPERIMENTAL RESULTS

### A. $\text{MnSc}_2\text{S}_4$

$\text{MnSc}_2\text{S}_4$  shows the usual thermal expansion at high temperatures. In Fig. 2(a), we show the relative length change,  $\Delta L/L$ , between 0.35 and 100 K. Below about 15 K magnetic contributions start to dominate  $\Delta L/L$ . We investigated the temperature dependence of  $\Delta L/L$  at various magnetic fields applied along  $[111]$ , as well as the magnetic-field dependence of the sample length up to 12 T at different temperatures (Fig. 3).

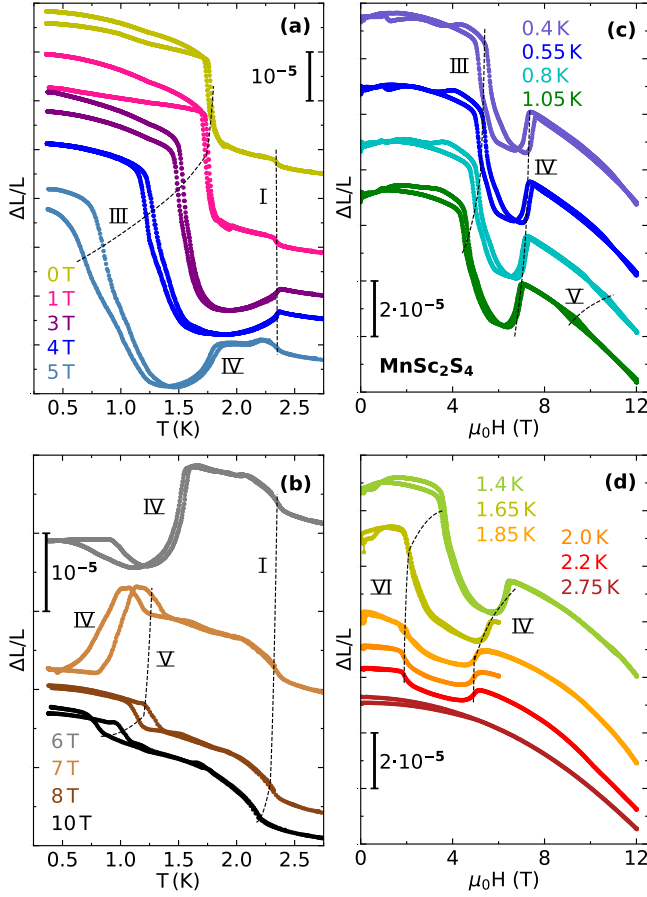


FIG. 3. (a), (b) Thermal expansion and (c), (d) magnetostriction of  $\text{MnSc}_2\text{S}_4$  single crystals for  $H \parallel \Delta L/L \parallel [111]$  after zero-field cooling (ZFC) from the paramagnetic state. The curves are shifted for better visibility. The black dashed lines indicate the phase transitions and are guides to the eye.

The thermal expansion [Figs. 3(a) and 3(b)] shows some clear anomalies, which we label by roman numbers. Two of them can be characterized at zero field at about 1.75 and 2.3 K. The latter (I) indicates the ordering temperature  $T_N$ . At 1.75 K (III), we find a huge magnetoelastic response. This transition is strongly field dependent and is visible up to about 5 T, where the anomaly broadens and becomes hysteretic. In the thermal-expansion coefficient  $\alpha = d(\Delta L/L)/dT$  we observe a weak but clear anomaly slightly above the transition III. This transition II appears at about 1.9 and 1.95 K at zero and 1 T, respectively [Fig. 2(b)]. Another anomaly appears at 5 T at 1.8 K (IV) as a length expansion with increasing temperature. This anomaly has a similar field dependence as transition III and can be followed up to 7 T. An additional hysteretic distortion (V) shows up at 7, 8, and 10 T near 1 K [Fig. 3(b)].

All these anomalies indicate phase transitions. Most of them are also present in magnetostriction data [Figs. 3(c) and 3(d)]. The transitions III and IV show a strong coupling to the lattice and form a valley-like region be-

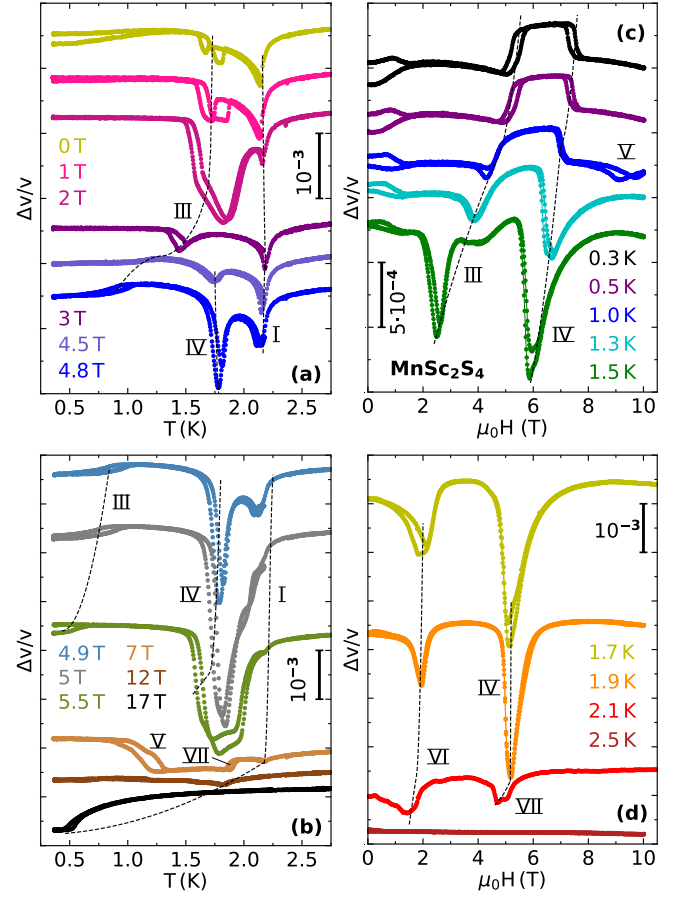


FIG. 4. Relative sound velocity of the longitudinal acoustic mode ( $\mathbf{k} \parallel \mathbf{u} \parallel \mathbf{H} \parallel [111]$ ,  $f = 81$  MHz) in  $\text{MnSc}_2\text{S}_4$  versus (a), (b) temperature and (c), (d) magnetic field, measured at selected temperatures and magnetic fields, respectively. The curves are shifted for better visibility. The black dashed lines indicate the phase transitions and are guides to the eye.

tween about 5 and 7 T at lowest temperatures. This is interesting, because skyrmions are predicted to appear in this field range [9], so this feature requires some further theoretical analysis (see discussion below). The valley remains up to 2.2 K, while it becomes less pronounced and nearly temperature independent above 1.65 K, shifting to a slightly changed phase above about 2 T (VI). The anomaly V can also be detected as a narrow hysteresis at higher fields. Finally, the data at 2.75 K are completely featureless, indicating paramagnetism.

We further performed measurements of the sound-velocity change as a function of temperature and magnetic field [Fig. 4], analogous to the dilatometry experiment. We excited a longitudinal mode along [111] with the magnetic field aligned in the same direction. Figures 4(a) and 4(b) show the relative change of the sound velocity  $\Delta v/v$  in  $\text{MnSc}_2\text{S}_4$  as a function of temperature for selected magnetic fields. We observe anomalies at similar temperatures as in our dilatometry measurements. The transition from the paramagnetic to the magnetically or-

dered state (I) appears as a clear minimum without any field dependence up to about 8 T. The transition III occurs as a broad hysteretic feature up to 2 T and changes into a narrow hysteresis that can be followed up to 5.5 T. We cannot resolve transition II in our ultrasound experiments, which might be caused by the hysteresis of transition III. The transition IV appears as a distinct dip that starts at 4.5 T and is visible up to 5.5 T as a sharp jump. Further, at 7 T, we observe a hysteresis in  $\Delta v/v$  at about 1.2 K, which we attribute to transition V. Another anomaly appears at this field at about 1.9 K (VII). The step-like feature at about 2 K in  $\Delta v/v$  at 5.5 T might be related to this transition as well.

We could observe most of the transitions as well in the field-dependent ultrasound experiments [Figs. 4(c) and 4(d)]. The transitions III and IV dominate the data, enclosing the previously observed skyrmion phase [9] as a plateau. Due to their weak temperature dependence, the transitions III and IV are sharper in field-dependent ultrasound (and magnetostriction) experiments. Like in magnetostriction, the shape of the plateau changes at higher temperatures. Jumps at low magnetic fields continuously turn into minima. The data at 1 K show a small hysteretic feature around 9 T corresponding to transition V. At 2.1 K, the anomalies IV and VII occur as a double dip at about 5 T, indicating the beginning of the phase line VII. Again at 2.5 K, above  $T_N$ ,  $\Delta v/v$  is completely featureless in the paramagnetic phase. Additionally, in Fig. 4(c) appears a hysteresis below about 1 K for measurements up to 1.5 K. This corresponds to domain orientation.

Both methods compared, it is important to note that the magnitude and shape of some transitions is different for magnetostriction and ultrasound, *e.g.* magnitudes of transitions IV and VI. Despite being lattice sensitive, both methods use different concepts to track lattice-effects. This leads to different sensitivities and overall shapes of the anomalies.

From the anomalies observed in the magnetoelastic data, we can construct the magnetic ( $H, T$ ) phase diagram for fields along [111], shown in Fig. 5. Our ultrasound and dilatometry data reveal a Néel temperature of 2.3 K. Due to the different measurement configurations, we see a small temperature difference within the experimental error of 5%. Error bars have been added to some of the affected triangles. The Néel temperature is ultimately in line with earlier susceptibility ( $T_N = 2.3$  K) [13] and specific-heat data with the peak at about 2.1 K [19]. Our temperature-dependent data allow to follow this phase transition I towards larger magnetic fields. Towards lower temperatures, we observe two further anomalies in the thermal expansion  $\alpha$  in zero field [Fig. 2(b)], in line with neutron-scattering data [8, 9]. The first transition (II) is very weak in  $\alpha$ , whereas transition III leads to a large lattice expansion towards lower temperatures [Figs. 2(b) and 3(a)]. The ultrasound data [Fig. 4(a)] show a pronounced hysteresis in this temperature region. The error bars shown in Fig. 5 reflect the

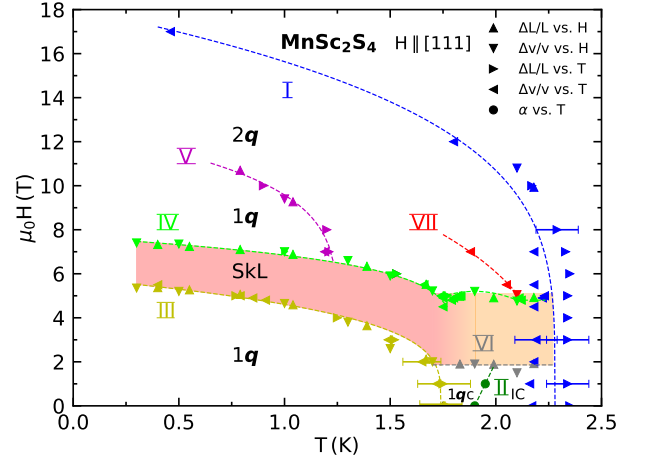


FIG. 5. Phase diagram of  $\text{MnSc}_2\text{S}_4$ . The numbers correspond to the labeling of the anomalies used in the text. The abbreviations indicate the magnetic structure of the phases (see also schematic pictures in [8]). The shape of the markers indicates the method used to extract the transitions.

width of this hysteresis.

In applied magnetic fields, our dilatometry and ultrasound data show anomalies at the phase transitions III and VI. These anomalies agree well with the transitions to the  $3q$  or antiferromagnetic skyrmionic phase observed in neutron scattering (red colored area in Fig. 5) [9].

At higher fields, above the skyrmion phase, two additional phase lines (V and VII) occur. The first one (V), below 1.2 K may separate a fan-single- $q$  structure from a  $2q$  structure. Our mean-field calculations, discussed later, suggest such a  $2q$  phase. The anomaly VII appears only in our ultrasound data. For this, we have no theoretical interpretation. It also seems that this line fades away towards lower temperatures and higher fields.

## B. $\text{MnSc}_2\text{Se}_4$

For  $\text{MnSc}_2\text{Se}_4$ , we performed as well dilatometry and ultrasound measurements as a function of temperature and magnetic field. Note that we used a single crystal of similar quality compared to  $\text{MnSc}_2\text{S}_4$ . Under similar experimental conditions, we observed that  $\text{MnSc}_2\text{Se}_4$  exhibits significantly fewer features than  $\text{MnSc}_2\text{S}_4$ . The temperature-dependent dilatometry measurements at various fixed magnetic fields reveal curves with negative slopes for moderate fields up to 5 T [Fig. 6(a)]. At higher fields, we find broad minima that shift to lower temperatures.

The field-dependent length changes [Fig. 6(c)] show negative slopes as well. As the temperature decreases, the magnetostrictive effect becomes stronger, indicating a quadratic parastriction that dominates over the thermal lattice vibrations. A model, based on exchange striction as the dominant interaction, can explain the negative



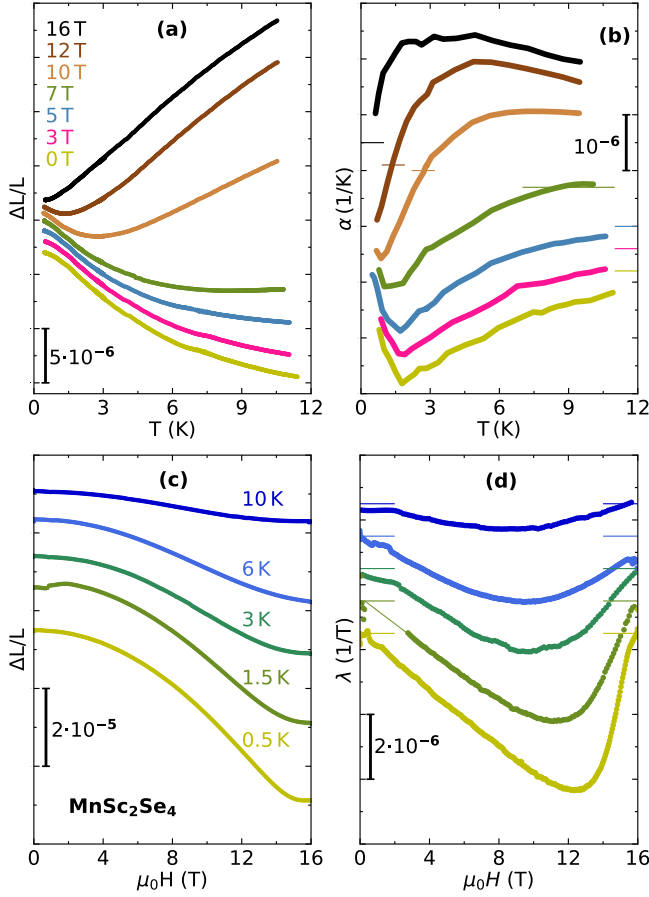


FIG. 6. Dilatometry data of  $\text{MnSc}_2\text{Se}_4$  in longitudinal geometry ( $\Delta L/L \parallel \mathbf{H} \parallel [111]$ ). (a) Thermal expansion and (b) its derivative, the thermal expansion coefficient  $\alpha$ . (c) Magnetostriction and (d) its derivative, the magnetostriction coefficient  $\lambda$ , up to 16 T. All curves are shifted for better visibility. The horizontal lines in the derivatives mark the zero point of the coefficient for the respective curve.

slope in both experiments [25].

In order to check for some minor, hidden anomalies, we calculated the derivatives  $\alpha$  [Fig. 6(b)] and  $\lambda = \frac{1}{\mu_0} \frac{d(\Delta L/L)}{dH}$  [Fig. 6(d)]. However, also the thermal-expansion coefficient  $\alpha$  is mostly featureless. For smaller fields, a broad minimum appears up to about 10 T. This minimum is temperature dependent, shifting from about 1.7 K at zero field to about 0.9 K at 10 T and is suppressed at 12 T. In the magnetostriction coefficient  $\lambda$ , a broad minimum appears as well, which shifts to higher magnetic fields with decreasing temperature. Ultimately, the dilatometry data show no clear anomaly that would indicate a phase transition.

We also measured the sound velocity changes as a function of  $T$  and  $H \parallel [111]$  for the longitudinal mode  $\mathbf{k} \parallel \mathbf{u} \parallel [111]$ . Figure 7(a) shows the relative change of the sound-velocity  $\Delta v/v$  in  $\text{MnSc}_2\text{Se}_4$  as a function of temperature for selected magnetic fields. For  $\text{MnSc}_2\text{Se}_4$ , we found anomalies in  $\Delta v/v$  in the order of  $10^{-3}$ . Here, we

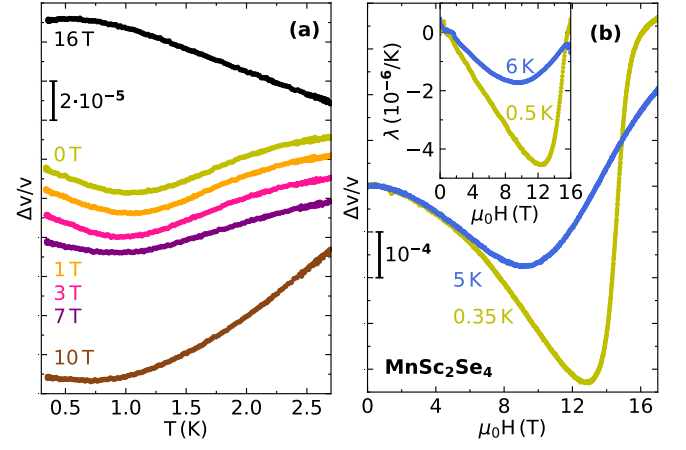


FIG. 7. (a) Temperature-dependent and (b) field-dependent sound-velocity change in  $\text{MnSc}_2\text{Se}_4$  for the longitudinal acoustic mode ( $\mathbf{k} \parallel \mathbf{u} \parallel \mathbf{H} \parallel [111]$ ,  $f = 81$  MHz) at selected magnetic fields [20]. The inset in (b) shows the magnetostriction coefficient  $\lambda = \partial/\partial B(\Delta L/L)$ , recorded at similar temperatures [see also Fig. 6(d)].

could not observe any sharp feature down to a resolution of some  $10^{-6}$ . In the temperature-dependent measurements, we observe a phonon softening down to about 1 K, which initially becomes larger with increasing magnetic field. At highest field (16 T), this dependence is reversed with a temperature-dependent hardening and saturation of  $\Delta v/v$  below about 0.7 K.

These results are in accordance with the sound-velocity data measured as a function of magnetic field [Fig. 7(b)]. At 0.35 K, we find a broad minimum at about 13 T. This minimum broadens and shifts to lower fields at higher temperatures. Soud *et al.* have discussed this behavior in detail previously [20]. When comparing these data with the magnetostriction coefficient  $\lambda$  in the inset of Fig. 7(b) [complete set of curves in Fig. 6(d)] the similar behavior of the broad anomalies is striking.

In order to search further for possible phase transitions in  $\text{MnSc}_2\text{Se}_4$ , we performed some additional thermodynamic investigations. We measured the specific heat in magnetic fields up to 14 T (Fig. 8). In zero field, the specific heat shows a broad anomaly at about 2 K. With increasing magnetic field, this feature becomes smaller, until it vanishes at about 12 T with the magnetic entropy shifting to higher temperatures. The specific-heat data evidence the absence of a magnetic phase transition down to 0.5 K.

We further measured the ac susceptibility in zero field at various excitation frequencies down to 1.5 K. The inverse ac susceptibility follows nicely a Curie-Weiss behavior at high temperatures, but deviates from the linear curve below about 20 K (Fig. 9). Such a deviation is characteristic for the existence of short-range (antiferromagnetic) correlations. The paramagnetic Curie-Weiss temperature is  $\Theta_{CW} = -15$  K and the effective moment is  $\mu_{eff} = 5.69 \mu_B$ . These values are in line with previ-

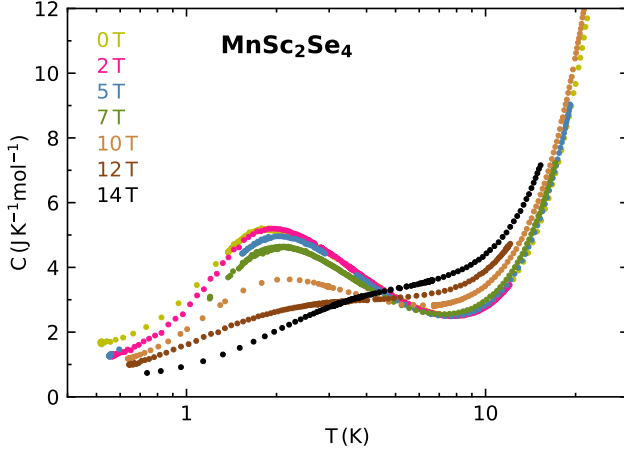


FIG. 8. Specific heat of  $\text{MnSc}_2\text{Se}_4$  in various fields applied along the [111] direction.

ously reported values of  $\Theta_{CW} = -18.4$  K and  $\mu_{eff} = 5.81 \mu_B$  extracted from ac-susceptibility data measured up to 400 K on a polycrystalline sample [7].  $\mu_{eff}$  is close to  $5.92 \mu_B$  for pure  $\text{Mn}^{2+}$   $S = 5/2$  spins.

The data show no frequency dependence between 0.5 and 3 kHz, which rules out spin-glass behavior. Our measurements would also agree with the existence of a spin-liquid state.

Comparing the results for both compounds, we find a largely different magnetic behavior. On the one hand, for  $\text{MnSc}_2\text{S}_4$ , we find a rich phase diagram including an antiferromagnetic skyrmion state above 2 to 5 T below about 2.3 K. In contrast,  $\text{MnSc}_2\text{Se}_4$  shows no indication of a phase transition down to 0.3 K and up to 16 T. The substitution of the smaller  $\text{S}^{2-}$  ions by the larger  $\text{Se}^{2-}$  ions seems to weaken the interatomic coupling between

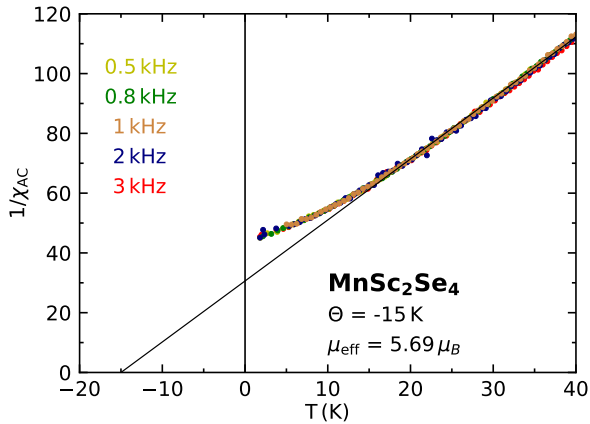


FIG. 9. Temperature-dependent inverse ac susceptibility of  $\text{MnSc}_2\text{Se}_4$  in zero field measured using various excitation frequencies of the ac field applied parallel to the [111] direction. The black line shows a linear fit to the data above 20 K.

the magnetic Mn ions, which prevents the formation of long-range order.

## IV. DISCUSSION

### A. $\text{MnSc}_2\text{S}_4$

In addition to experimental investigations, we used the mean-field simulation program MCPHASE [26] to rationalize the strong magnetoelastic response to skyrmions. We extended the theory introduced by Gao *et al.* [9] by an elastic-energy term to calculate the lattice expansion. We set up a model taking into account only effects of exchange striction, since we expect only very weak second-order crystal-field effects for the  $\text{Mn}^{3+}$  ions. Based on our notation the Hamiltonian appears as

$$\begin{aligned} \mathcal{H} &= \mathcal{H}_0 + \mathcal{H}_{\parallel} + \mathcal{H}_A + \mathcal{H}_Z + E_{el} \\ &= -\frac{1}{2} \sum_{ij} J(\mathbf{r}_{ij}) \mathbf{S}_i \cdot \mathbf{S}_j \\ &\quad - \frac{1}{2} J_{\parallel} \sum_{ij \in NN} \frac{1}{|\mathbf{r}_{ij}|^2} (\mathbf{S}_i \cdot \mathbf{r}_{ij})(\mathbf{r}_{ij} \cdot \mathbf{S}_j) \\ &\quad + A_4 \sum_{i, \alpha=x,y,z} (S_i^{\alpha})^4 - g\mu_B \mu_0 \sum_i \mathbf{H} \cdot \mathbf{S}_i \\ &\quad + \frac{V}{2} \sum_{\alpha\alpha'\beta\beta'} c^{\alpha\alpha'\beta\beta'} \varepsilon_{\alpha\alpha'} \varepsilon_{\beta\beta'}, \end{aligned} \quad (1)$$

with the coupling constants according with [9]  $J_1 = 0.053$  meV,  $J_2 = -0.079$  meV,  $J_3 = -0.015$  meV, and the anisotropic coupling strength  $J_{\parallel} = 0.005$  meV and the single ion anisotropy constant  $A_4 = 0.14 \mu\text{eV}$ .  $\mathbf{H}$  is the external magnetic field,  $\mathbf{S}_i$  is the spin of ion  $i$  in units of  $\hbar$ , and  $\mathbf{r}_{ij}$  is the connection vector between ions  $i$  and  $j$ . We derive a set of equations for the strain components  $\varepsilon_{\beta\beta'}$  by including the strain dependence of the exchange interactions and minimizing the free energy with respect to  $\varepsilon_{\beta\beta'}$ . The result is

$$\begin{aligned} \sum_{\beta, \beta'=1\dots 3} c^{\alpha\alpha'\beta\beta'} \varepsilon_{\beta\beta'} &= \\ \frac{1}{4V} \sum_{ij} \left( r_{\alpha} \frac{\partial J(\mathbf{r}_{ij})}{\partial r_{\alpha'}} + r_{\alpha'} \frac{\partial J(\mathbf{r}_{ij})}{\partial r_{\alpha}} \right) \langle \mathbf{S}^i \cdot \mathbf{S}^j \rangle, \end{aligned} \quad (2)$$

which, in general, represents six independent equations.  $\langle \mathbf{S}^i \cdot \mathbf{S}^j \rangle$  is the scalar product of neighboring spin moments. The non-zero components of the symmetric elastic-constants tensor  $c^{\alpha\alpha'\beta\beta'}$  were calculated by the use of an empirical Born von Karmán model as

$$\begin{aligned} c^{\alpha\alpha\alpha\alpha} &= 93 \text{ GPa} \\ c^{\alpha\alpha\beta\beta} &= c^{\alpha\beta\alpha\beta} = 29 \text{ GPa}, \end{aligned} \quad (3)$$

with new components  $\alpha, \beta = 1, 2, 3$  and  $\alpha \neq \beta$ . In order to calculate  $\partial J(\mathbf{r}_{ij}) / \partial r_{ij}^{\alpha'}$  we introduced a parametrization [27] for  $J(\mathbf{r}_{ij})$  based on  $J_1$ ,  $J_2$ , and  $J_3$  given by

$$J(\mathbf{r}_{ij}) = A (r_0^2 - r_0^4) e^{-\gamma r_0^2}, \quad (4)$$

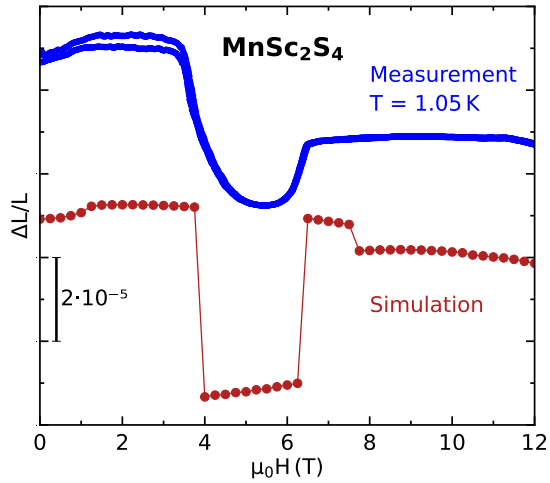


FIG. 10. Simulated magnetostriction (red) of  $\text{MnSc}_2\text{S}_4$  using MCPHASE with fields applied along the  $[111]$  direction compared to the measured magnetostriction at 1.05 K (blue) with subtracted phononic background (magnetostriction data measured at 2.75 K, see Fig. 3).

with  $r_0 = |\mathbf{r}_{ij}|/R$  and obtained the corresponding constants  $A = 4.864$  meV,  $R = 4.740$  Å, and  $\gamma = 2.450$ .

We compare the data of simulation and experiment of the magnetic contribution to the magnetostriction in Fig. 10. The qualitative agreement between theory and experiment is striking. The sequence of transitions is the same for the calculated propagation vectors. At zero field and very low temperatures, the simulation results in a single- $\mathbf{q}$  state with propagation vector  $(3/4, 3/4, 0)$ , corresponding to a helical structure with nonsymmetric domains [28]. A transition to a  $3\mathbf{q}$  state appears at about 4 T, corresponding to the skyrmion lattice. This transition shows a strong magnetoelastic response. Above about 6 T, we find another single- $\mathbf{q}$  structure with the same propagation as the former. Based on the calculation, both single- $\mathbf{q}$  phases are similar, but our measurements show a clear difference in the lattice expansion, indicating a different, most likely fan-like single- $\mathbf{q}$  phase. Finally, the simulation shows a step in  $\Delta L/L$  around 7.5 T, which fits to the transition V. The neutron-scattering intensities of the simulated propagations suggest that this new phase has a  $2\mathbf{q}$  structure.

We can explain the strong lattice contraction in the  $3\mathbf{q}$  skyrmion phase directly from the linear dependence of strain and nearest-neighbor correlation  $\langle \mathbf{S}^i \cdot \mathbf{S}^j \rangle$  in Eq. (2). In the  $3\mathbf{q}$  state, each magnetic moment is aligned almost parallel to the neighboring moment, only rotated by a small twist angle. In the single- $\mathbf{q}$  state, on the other hand, each magnetic moment has two nearly parallel neighbors in the propagation direction and four neighbors with antiparallel contributions, due to the overall antiferromagnetic coupling. This leads to a jump in the nearest-neighbor correlation at the transition from the single- $\mathbf{q}$  to the  $3\mathbf{q}$  state, which directly influences the

magnetostriction, as seen in our experiments and simulations. The slightly smaller  $\Delta L/L$  for the single- $\mathbf{q}$  phase above transition IV compared to the ground state is in line with the observed fan state at higher fields [9] according to the explanation by nearest-neighbor correlations. This small difference occurs because the moments of neighboring Mn ions are aligned less antiparallel to each other in the fan state compared to the helical ground state.

## B. $\text{MnSc}_2\text{Se}_4$

In contrast to  $\text{MnSc}_2\text{S}_4$  we could not find long-range magnetic order in  $\text{MnSc}_2\text{Se}_4$ , which contradicts the neutron-scattering results on powder samples [7]. This may be caused by internal stresses in single crystals compared to the powder samples. Here, we can show that an explanation that allows a helical ground state is also possible. The broad maximum in the specific heat may indicate the lack of a distinct energy scale. This is typical for systems with disorder or randomness, which may be caused by random site exchanges of the cations (antisite defects), which is often the case in Se systems [29–31]. Introducing randomness in this way is used since more than 50 years [32]. These site exchanges between Mn and Sc (local disorder) are energetically favorable also in  $\text{MnSc}_2\text{Se}_4$  crystals. Due to different internal distortions, the distance of neighboring Mn sites might vary. In consequence, the exchange interactions vary as well. All together, larger bond lengths and antisite-defects are connected to each other and cannot be separated experimentally.

However, in our simulation we can tune the amount of defects, which allows us to find hints which effect causes the different behavior. In particular, we performed a calculation of the specific heat based on the exchange interactions  $J_1$ ,  $J_2$ , and  $J_3$ . We assumed a Gaussian variation of the exchange coupling with mean values  $J_i$  ( $i = 1, 2, 3$ ) and standard deviation  $W$  for each exchange. This approach to model the antisite defects is not possible with MCPHASE. Instead, we used the Metropolis algorithm to perform Monte Carlo calculations of a classical Heisenberg model with interactions up to the third nearest neighbor. Our simulations are similar to former calculations [33, 34]. We set the mean coupling constants to the optimal values obtained from fits to the magnon dispersion ( $J_1 = 0.050$  meV,  $J_2 = -0.062$  meV,  $J_3 = -0.008$  meV) [7]. We determined the specific heat from the energy variance.

At zero magnetic field, the pure system with zero standard deviation ( $W = 0$ ) shows a sharp divergent peak in the specific heat at a first-order phase transition with  $T_N \approx 2$  K. This would evidence long-range order. Increasing randomness of the exchange broadens the specific-heat peak and the finite-temperature phase transition disappears above a threshold of  $W$  between 0.04 and 0.08 K. We chose  $W = 0.18$  K to best reproduce the

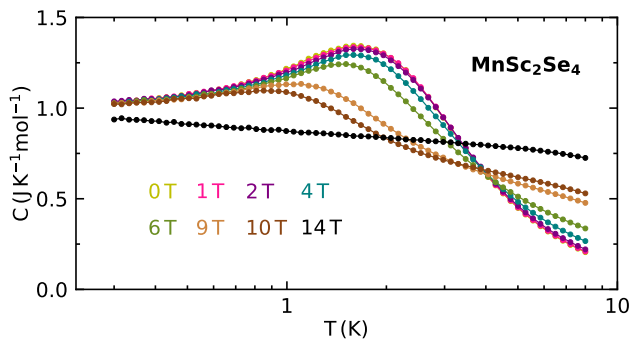


FIG. 11. Magnetic specific heat of  $\text{MnSc}_2\text{Se}_4$  obtained by Monte Carlo simulations of a  $J_1$ - $J_2$ - $J_3$  model with a bond randomness parameter  $W$  with fields applied along [111].

peak width of the experimentally measured specific heat (Fig. 8). We show the calculated data for several magnetic fields in Fig. 11. Note that the measured specific heat in Fig. 8 still includes the contribution from phonons, contrary to the Monte Carlo results. The calculated field and temperature dependence of the specific heat qualitatively agrees with the experimental data. This agreement indicates that bond randomness may be significant in  $\text{MnSc}_2\text{Se}_4$  and avoids an overall helical ground state. Increased bond lengths alone would allow a sharp transition to long range magnetic order, based on our simulation. We cannot decide, if magnetic structures, like the SkL would also occur without bond-randomness. But this is quite speculative, since there is no possibility to exclude antisite-defects in  $\text{MnSc}_2\text{Se}_4$ .

## V. SUMMARY

We investigated the spinel compounds  $\text{MnSc}_2\text{X}_4$  ( $X = \text{S}, \text{Se}$ ) by using ultrasound and dilatometry experiments, supported by further thermodynamic methods as well as model calculations. For single-crystalline  $\text{MnSc}_2\text{S}_4$ , we constructed a rich  $(H, T)$  phase diagram based on the anomalies found in the ultrasound and dilatometry data. At zero field, our data indicate the existence of three magnetic phases in line with earlier results [8, 9]. A commensurate single- $q$  helical ground state at lowest temperature has been proposed, which is followed by an intermediate incommensurate state and a collinear state prior to the transition into paramagnetism. In magnetic

fields applied along [111], we observe clear anomalies evidencing the phase transitions to the  $3q$  skyrmion phase seen in neutron scattering [9]. This skyrmion phase is restricted to a roughly 2 T broad region. It turns out that the skyrmions couple strongly to the lattice and induce pronounced effects in the magnetoelastic properties. This is similar to other compounds, *e.g.* the 4f-magnet  $\text{Gd}_2\text{PdSi}_3$  [35] or  $\text{FeGe}$  [36], including volume variations. We further observe two new phase-transition lines in  $\text{MnSc}_2\text{S}_4$ , one of which may separate a  $2q$  phase.

For  $\text{MnSc}_2\text{Se}_4$ , on the other hand, we could not detect any sharp phase transition. Only a broad peak in the specific heat appears at about 2 K. This may indicate a spin-liquid state. However, assuming some randomness in the lattice, due to larger bond lengths, our Monte Carlo calculations can explain the broad specific-heat peak and still support the possibility of a helical ground state. Nevertheless, unlike  $\text{MnSc}_2\text{S}_4$ ,  $\text{MnSc}_2\text{Se}_4$  does not contain a skyrmionic state.

Further intriguing changes in the magnetic properties might occur with complete or partial substitutions on the Sc or X sites, which may clarify further details about the Mn spinels.

## ACKNOWLEDGMENTS

We acknowledge support from Deutsche Forschungsgemeinschaft (DFG) through SFB 1143 (Project-ID 247310070), the Würzburg-Dresden Cluster of Excellence on Complexity and Topology in Quantum Matter—*ct.qmat* (EXC 2147, Project No. 390858490), and TRR 360 (Project No. 492547816). We as well acknowledge the support of the HLD at HZDR, member of European Magnetic Field Laboratory (EMFL). We thank Oksana Zaharko for fruitful discussions. L.P. and V.T. thank for support by the project ANCD (code 011201, Moldova). H.S. acknowledges support from JSPS KAKENHI Grant Nos. JP22K03508 and JP24H01609. Monte Carlo calculations were performed using computational resources of the Supercomputer Center at the Institute for Solid State Physics, the University of Tokyo.

## DATA AVAILABILITY

The data that support the findings of this article are openly available Ref. [37].

- 
- [1] V. Tsurkan, H.-A. K. von Nidda, J. Deisenhofer, P. Lunkenheimer, and A. Loidl, On the complexity of spinels: Magnetic, electronic, and polar ground states, *Phys. Rep.* **926**, 1 (2021).
  - [2] A. S. Cameron, Y. V. Tymoshenko, P. Y. Portnichenko, J. Gavilano, V. Tsurkan, V. Felea, A. Loidl, S. Zherlitsyn, J. Wosnitzer, and D. S. Inosov, Magnetic phase diagram

of the helimagnetic spinel compound  $\text{ZnCr}_2\text{Se}_4$  revisited by small-angle neutron scattering, *J. Phys.: Condens. Matter* **28**, 146001 (2016).

- [3] P. Zajdel, W.-Y. Li, W. van Beek, A. Lappas, A. Ziolkowska, S. Jaskiewicz, C. Stock, and M. A. Green, Structure and magnetism in the bond-frustrated spinel  $\text{ZnCr}_2\text{Se}_4$ , *Phys. Rev. B* **95**, 134401 (2017).



- [4] D. S. Inosov, Y. O. Onyikienko, Y. V. Tymoshenko, A. Akopyan, D. Shukla, N. Prasai, M. Doerr, D. Gorbunov, S. Zherlitsyn, D. J. Voneshen, M. Boehm, V. Tsurkan, V. Felea, A. Loidl, and J. L. Cohn, Magnetic field dependence of low-energy magnons, anisotropic heat conduction, and spontaneous relaxation of magnetic domains in the cubic helimagnet  $\text{ZnCr}_2\text{Se}_4$ , *Phys. Rev. B* **102**, 184431 (2020).
- [5] D. Bergman, J. Alicea, E. Gull, S. Trebst, and L. Balents, Order-by-disorder and spiral spin-liquid in frustrated diamond-lattice antiferromagnets, *Nat. Phys.* **3**, 487 (2007).
- [6] F. L. Buessen, M. Hering, J. Reuther, and S. Trebst, Quantum spin liquids in frustrated spin-1 diamond antiferromagnets, *Phys. Rev. Lett.* **120**, 057201 (2018).
- [7] K. Guratinder, V. Tsurkan, L. Prodan, L. Keller, J. P. Embs, F. Juranyi, M. Medarde, C. Rüegg, and O. Zaharko, Magnetic order and exchange coupling in the frustrated diamond-lattice antiferromagnet  $\text{MnSc}_2\text{Se}_4$ , *Phys. Rev. B* **105**, 174423 (2022).
- [8] S. Gao, O. Zaharko, V. Tsurkan, Y. Su, J. S. White, G. S. Tucker, B. Roessli, F. Bourdarot, R. Sibille, D. Chernyshov, T. Fennell, A. Loidl, and C. Rüegg, Spiral spin-liquid and the emergence of a vortex-like state in  $\text{MnSc}_2\text{Se}_4$ , *Nat. Phys.* **13**, 157 (2017).
- [9] S. Gao, H. D. Rosales, F. A. Gómez Albarracín, V. Tsurkan, G. Kaur, T. Fenell, P. Steffens, M. Boehm, P. Cermak, A. Schneidewind, E. Ressouche, D. C. Cabra, C. Rüegg, and O. Zaharko, Fractional antiferromagnetic skyrmion lattice induced by anisotropic couplings, *Nature* **586**, 37 (2020).
- [10] H. D. Rosales, F. A. Gómez Albarracín, K. Guratinder, V. Tsurkan, L. Prodan, E. Ressouche, and O. Zaharko, Anisotropy-driven response of the fractional antiferromagnetic skyrmion lattice in  $\text{MnSc}_2\text{Se}_4$  to applied magnetic fields, *Phys. Rev. B* **105**, 224402 (2022).
- [11] T. Kurumaji, T. Nakajima, M. Hirschberger, A. Kikkawa, Y. Yamasaki, H. Sagayama, H. Nakao, Y. Taguchi, T.-h. Arima, and Y. Tokura, Skyrmion lattice with a giant topological hall effect in a frustrated triangular-lattice magnet, *Science* **365**, 914–918 (2019).
- [12] N. D. Khanh, T. Nakajima, X. Yu, S. Gao, K. Shibata, M. Hirschberger, Y. Yamasaki, H. Sagayama, H. Nakao, L. Peng, K. Nakajima, R. Takagi, T.-h. Arima, Y. Tokura, and S. Seki, Nanometric square skyrmion lattice in a centrosymmetric tetragonal magnet, *Nat. Nanotechnol.* **15**, 444–449 (2020).
- [13] A. Krimmel, M. Mücksch, V. Tsurkan, M. M. Koza, H. Mutka, C. Ritter, D. V. Sheptyakov, S. Horn, and A. Loidl, Magnetic ordering and spin excitations in the frustrated magnet  $\text{MnSc}_2\text{Se}_4$ , *Phys. Rev. B* **73**, 014413 (2006).
- [14] Y. Iqbal, T. Müller, H. O. Jeschke, R. Thomale, and J. Reuther, Stability of the spiral spin liquid in  $\text{MnSc}_2\text{Se}_4$ , *Phys. Rev. B* **98**, 064427 (2018).
- [15] S. Giri, H. Nakamura, and T. Kohara, Classical antiferromagnetism in  $\text{MnSc}_2\text{Se}_4$ : A  $^{45}\text{Sc}$  NMR study, *Phys. Rev. B* **72**, 132404 (2005).
- [16] G. M. Kalvius, O. Hartmann, D. R. Noakes, F. E. Wagner, R. Wäppling, U. Zimmermann, C. Baines, A. Krimmel, V. Tsurkan, and A. Loidl, A  $\mu\text{SR}$  magnetic study of frustrated  $\text{FeSc}_2\text{S}_4$  and  $\text{MnSc}_2\text{S}_4$ , *Physica B* **378–380**, 592 (2006).
- [17] K. Momma and F. Izumi, *VESTA3* for three-dimensional visualization of crystal, volumetric and morphology data, *J. Appl. Crystallogr.* **44**, 1272 (2011).
- [18] L. Pawlak and M. Duczmal, Magnetic and structural properties of scandium chalcogenide spinels with iron and manganese, *Int. J. Mod. Phys. B* **07**, 1020 (1993).
- [19] V. Fritsch, J. Hemberger, N. Büttgen, E.-W. Scheidt, H.-A. Krug von Nidda, A. Loidl, and V. Tsurkan, Spin and Orbital Frustration in  $\text{MnSc}_2\text{S}_4$  and  $\text{FeSc}_2\text{S}_4$ , *Phys. Rev. Lett.* **92**, 116401 (2004).
- [20] J. Sourd, Y. Skourski, L. Prodan, V. Tsurkan, A. Miyata, J. Wosnitza, and S. Zherlitsyn, Magnon-phonon interactions in the spinel compound  $\text{MnSc}_2\text{Se}_4$ , *Phys. Rev. B* **110**, 094414 (2024).
- [21] R. Küchler, T. Bauer, M. Brando, and F. Steglich, A compact and miniaturized high resolution capacitance dilatometer for measuring thermal expansion and magnetostriction, *Rev. Sci. Instrum.* **83**, 095102 (2012).
- [22] B. Lüthi, *Physical Acoustics in the Solid State* (Springer, 2005).
- [23] A. Hauspurg, S. Zherlitsyn, T. Helm, V. Felea, J. Wosnitza, V. Tsurkan, K.-Y. Choi, S.-H. Do, M. Ye, W. Brenig, and N. B. Perkins, Fractionalized excitations probed by ultrasound, *Phys. Rev. B* **109**, 144415 (2024).
- [24] T. H. K. Barron and G. K. White, *Heat Capacity and Thermal Expansion at Low Temperatures* (Springer, 1999).
- [25] M. Doerr, M. Rotter, and A. Lindbaum, Magnetostriction in rare-earth based antiferromagnets, *Adv. Phys.* **54**, 1 (2005).
- [26] M. Rotter, McPhase manual (2025), <https://mcphase.github.io/webpage/manual/manual.html>.
- [27] T. Kaneyoshi, A molecular field theory of amorphous ferromagnets, *J. Phys. C: Solid State Phys.* **6**, 3130 (1973).
- [28] M. Hirschberger, T. Nakajima, S. Gao, L. Peng, A. Kikkawa, T. Kurumaji, M. Kriener, Y. Yamasaki, H. Sagayama, H. Nakao, K. Ohishi, K. Kakurai, Y. Taguchi, X. Yu, T. hisa Arima, and Y. Tokura, Skyrmion phase and competing magnetic orders on a breathing kagomé lattice, *Nat. Commun.* **10**, 13675 (2019).
- [29] D. W. Houck, E. I. Assaf, H. Shin, R. M. Greene, D. R. Pernik, and B. A. Korgel, Pervasive Cation Vacancies and Antisite Defects in Copper Indium Diselenide ( $\text{CuInSe}_2$ ) Nanocrystals, *J. Phys. Chem. C* **123**, 9544 (2019).
- [30] S.-H. Wei and S. Zhang, Defect properties of  $\text{CuInSe}_2$  and  $\text{CuGaSe}_2$ , *J. Phys. Chem. Solids* **66**, 1994 (2005).
- [31] P. Canepa, G. Sai Gautam, D. Broberg, S.-H. Bo, and G. Ceder, Role of point defects in spinel mg chalcogenide conductors, *Chem. Mater.* **29**, 9657 (2017).
- [32] S. Ben-Abraham, On internal stresses due to a random distribution of dislocations, *Scr. Metall.* **2**, 9 (1968).
- [33] A. Miyata, H. Suwa, T. Nomura, L. Prodan, V. Felea, Y. Skourski, J. Deisenhofer, H.-A. Krug von Nidda, O. Portugall, S. Zherlitsyn, V. Tsurkan, J. Wosnitza, and A. Loidl, Spin-lattice coupling in a ferrimagnetic spinel: Exotic  $H - T$  phase diagram of  $\text{MnCr}_2\text{S}_4$  up to 110 K, *Phys. Rev. B* **101**, 054432 (2020).
- [34] M. Gen and H. Suwa, Nematicity and fractional magnetization plateaus induced by spin-lattice coupling in the classical kagome-lattice Heisenberg antiferromagnet, *Phys. Rev. B* **105**, 174424 (2022).
- [35] S. Spachmann, A. Elghandour, M. Frontzek, W. Löser, and R. Klingeler, Magnetoelastic coupling and phases

- in the skyrmion lattice magnet  $\text{Gd}_2\text{PdSi}_3$  discovered by high-resolution dilatometry, *Phys. Rev. B* **103**, 184424 (2021).
- [36] M. Mito, T. Tajiri, Y. Kousaka, M. Miyagawa, T. Koyama, J. Akimitsu, and K. Inoue, Magnetostriction related to skyrmion-lattice formation in chiral magnet FeGe, *J. Appl. Phys.* **136**, 123902 (2024).
- [37] J. Grumbach, J. Sourd, M. Deeb, A. Miyata, H. Suwa, T. Gottschall, A. Hauspurg, S. Chattopadhyay, M. Rotter, S. Granovsky, L. Prodan, V. Tsurkan, S. Zherlitsyn, M. Doerr, and J. Wosnitza, Data underpinning: Contrasting magnetic behavior in  $\text{MnSc}_2\text{X}_4$  ( $X = \text{S}, \text{Se}$ ) spinel compounds investigated by magnetoelastic studies (2025), <https://datashare.tu-dresden.de/s/Fptpic3Exyn3pBL>, Accessed: 2025-09-04.